Efficient methodology for seismic fragility curves estimation by active learning on Support Vector Machines

Rémi Sainct, Cyril Feau, Jean-Marc Martinez, Josselin Garnier

Version of Record: https://www.sciencedirect.com/science/article/pii/S0167473020300515
Manuscript_30bddcd3a5bf0f9ec2af2dd0b3cc3dea

Efficient methodology for seismic fragility curves estimation by Active Learning on Support Vector Machines

Rémi Sainct[a], Cyril Feau[a,*], Jean-Marc Martinez[b], Josselin Garnier[c]

[a] *DES/ISAS-Service d'études mécaniques et thermiques (SEMT), CEA, Université Paris-Saclay, F-91191 Gif-sur-Yvette, France*
[b] *DES/ISAS-Service de thermo-hydraulique et de mécanique des fluides (STMF), CEA, Université Paris-Saclay, F-91191 Gif-sur-Yvette, France*
[c] *CMAP, Ecole Polytechnique, 91128 Palaiseau Cedex, France*

Abstract

Fragility curves which express the failure probability of a structure as function of a loading intensity measure are nowadays widely used to facilitate the design and decision making of structures/infrastructures against seismic hazard (and possibly other natural hazards), with analysis procedures specified by Seismic Probabilistic Risk Assessment, Performance-Based Earthquake Engineering, and other frameworks. To avoid the use of parametric models (such as the lognormal model) to estimate fragility curves from a reduced number of numerical calculations, a methodology based on Support Vector Machines (SVMs) coupled with an active learning algorithm is proposed in this paper. In practice, input excitation is reduced to some relevant parameters and then SVMs are used for a binary classification of the structural responses relative to a limit threshold of exceedance. Since the output is not binary but a real-valued score, a probabilistic interpretation of the output is exploited to estimate very efficiently fragility curves as score functions or as functions of classical seismic intensity measures.

Keywords: Fragility curve, Active Learning, Support Vector Machines, seismic intensity measure indicator

*Corresponding author
Email addresses: remi.sainct@m4x.org (Rémi Sainct), cyril.feau@cea.fr (Cyril Feau), jean-marc.martinez@cea.fr (Jean-Marc Martinez), josselin.garnier@polytechnique.edu (Josselin Garnier)

1. Introduction

In Seismic Probabilistic Risk Assessment (SPRA, e.g. [1]) as well as in Performance-Based Earthquake Engineering (PBEE, e.g. [2, 3]) frameworks, a key point is the evaluation of fragility curves which express the failure probability of a structure (or critical components) as a function of a seismic Intensity Measure (IM) such as the Peak Ground Acceleration (PGA) or the Pseudo-Spectral Acceleration (PSA). Apart from the use in SPRA and PBEE frameworks, fragility curves are useful for making decisions regarding the choice of construction details, to improve the structural performance of installations under seismic excitations [4, 5, 6, 7] or hurricanes [8]. They are also used to evaluate the role of the ground motion characteristics (near-fault type like, broadband, e.g. [7, 9]), of the soil-structure interaction [10] or of the numerical modeling assumptions [11] etc. Beyond the seismic hazard, fragility curves are also used for wind hazards [8, 12].

In theory, for complex structures, fragility curves have to be evaluated empirically based on a large number of mechanical analyses requiring, in most cases, nonlinear time-history calculations including both the uncertainties inherent to the system capacity and to the seismic demand, respectively called epistemic and aleatory uncertainties [1, 13, 14]. Nevertheless, the prohibitive computational cost induced by most nonlinear mechanical models requires the development of numerically efficient methods to evaluate such curves from a limited number of computations.

Following the idea proposed in the early 1980's in the framework of nuclear safety assessment [1], the lognormal parametric model was widely used in many applications to estimate fragility curves from a limited number of numerical calculations [4, 5, 6, 9, 10, 13, 15, 16, 17, 18, 19]. Different methods can be employed to determine or estimate the parameters of the lognormal model [15, 16, 20, 21] as well as different model assumptions [18, 19, 22]. However, the validity of the parametric models is itself questionable [18, 19, 21, 22, 23].

In practice, as it is very difficult to verify the validity of a parametric model assumption, the need of a numerically efficient non-parametric-based methodology (which would be accurate with a limited number of mechanical analyses) is necessary. One way to achieve this goal is to build a metamodel (i.e. a surrogate model of the mechanical analysis) which expresses the sta-

tistical relation between seismic inputs and structural outputs also called Engineering Demand Parameters (EDP). Various metamodeling strategies have been proposed recently in the literature based on, for example, response surfaces [24, 25], kriging [7] and Artificial Neural Networks (ANNs) [26]. In [8], considering storage tanks subjected to hurricane induced storm surge, prediction accuracy of three metamodels (SVMs, Random Forest and Logistic Regression) was systematically assessed and compared for various failure modes and Logistic Regression models were found to be the most accurate in order to estimate fragility curves.

The goal of this paper is twofold. First, it proposes a simple and efficient methodology for estimating non-parametric fragility curves that allows to reduce the number of mechanical numerical simulations by optimizing their selection. Second, it addresses the question of the best seismic IM indicator that can be used as the abscissa of the fragility curves and that can be defined as a simple function of a set of macroscopic IMs. This set includes but is not limited to PGA and PSA. Although the search for an optimal IM indicator is not strictly part of a fragility analysis, it is not disconnected from the first goal in particular in the framework of metamodeling strategies since the performance of a metamodel depends on the IM used. Consequently, many researchers have addressed this issue in the context of performance-based engineering assessments, see e.g. [19, 27, 28, 29, 30, 31]. With the strategy implemented in this work the two problems can be addressed together since the SVM output is not binary but a real-valued score (SVM margin) and a probabilistic interpretation of this score can be introduced to estimate score-based fragility curves.

Regarding the question of the IM indicators, a complete review of those proposed in the literature can be found in [19] as well as five optimality criteria (efficiency, practicality, proficiency, sufficiency and hazard computability successively introduced in [27, 28, 29, 31]). According to these criteria, the methodology proposed here consists in defining a proficient IM, proficiency being a composite measure of efficiency and practicality. Indeed, the score function can be viewed as an efficient IM since a perfect classifier would lead to a fragility curve in the form of a unit step function when the problem is linearly separable. Moreover, as it is highly correlated with the EDP, it can be considered as a practical IM. Hazard compatibility and sufficiency are out of the scope of this paper.

In contrast to classical learning (passive learning), the active learner selects the most useful numerical experiments to be carried out and added to

the learning data set. The "learner" chooses the best instances from a given very large set of unlabeled examples. So, the main question in active learning is how to choose new numerical experiments to be labeled. Various methods proposed in active learning by ANNs are presented in [32], which are typically based on several "learners" [33, 34]. With SVMs, active learning can be done easily by using only one "learner" because the distance to the separator hyperplane is a natural criterion for selecting new points to label [35]. A similar technique using logistic output ANNs can be used by analyzing the logit of the output. But in this case, given the non-linearity of the ANNs, the different learnings of the learner may present a strong variability on the decision boundary.

The recent progress on the simulation of seismic ground motions makes it possible to propose an active learning-based methodology, which requires a number of realizations larger than the size of the available real signals databases (in order to optimize their selection), but small enough to be able to use complex mechanical models. Various techniques can be used to create artificial seismic signals (e.g. the review presented in [36] and non-exhaustive references [23, 37, 38, 39, 40]). In this work, we have chosen to enrich a set of acceleration records selected in a real ground motion database using magnitude and distance criteria. To this end, the parameterized stochastic model of modulated and filtered white-noise process defined in [41] was implemented. This model efficiently addresses both temporal and spectral nonstationarities of seismic signals and has been used in several recent works [21, 42, 43, 44, 45]. The advantage of this model is that its constitutive parameters that characterize its time-frequency envelope can be considered as input parameters of a metamodel additionnaly with the classical IM parameters (PGA, PSA, etc.). Indeed, although the links between the Ground Motion Simulation Model's (GMSM's) parameters and the nonlinear structural responses are complex, intrinsically these parameters contain information that can help to discriminate seismic signals from the point of view of their damaging potential. A machine learning-based approach allows to capture such unintuitive links.

The methodology proposed to estimate fragility curves consists first of all in generating a large set of artificial seismic signals and to compute the different IM indicators of interest. In practice, this step is not time consuming in contrast with the nonlinear mechanical calculations. Then, the second step consists in building a SVM-based classifier by optimally selecting by active learning the mechanical calculations to perform. A probabilistic interpretation of the real-valued score given by the classifier is used in a third step to

estimate score-based fragility curves. The classifier can also be used to predict the scores and probabilities associated to new input parameters in order to estimate fragility curves as functions of the classical seismic IMs. These new input parameters can be the ones of the artifical signals that have not been selected for the construction of the classifier, or new ones generated by new simulations of the GMSM, or new ones that come from new real seismic signals (the procedure proposed in [41, 46] makes it possible to extract the input parameters of any real signal). Different procedures can be used to construct empirical fragility curves [3, 21, 23]. Here we propose a method based on k-means clustering of the IM data [23]. This means that in each cluster, the probability of failure corresponds to the ratio between the number of structural responses that exceed the limit threshold and the number of structural responses belonging to the cluster.

In this paper, the GMSM implemented for this work is briefly presented in section 2. In order to validate the methodology within a direct Monte Carlo-based approach, a simple inelastic oscillator is considered. This structural model is presented in section 2 as well as the IM indicators. Section 3 is devoted to the presentation of different classification methods and the active learning algorithm. Section 4 explains how the proposed methodology is used to estimate fragility curves, using either the score functions or the classical IM indicators. The conclusion is presented in section 5.

2. Ground Motion Simulation Model, Mechanical Structure Model, and Intensity Measure Indicators

In this section, the GMSM implemented for this work is briefly presented, followed by the model of the mechanical structure which is used to illustrate the methodology, and the choice of the IM indicators selected as inputs of the classifiers. A discussion is finally proposed about the GMSMs.

2.1. Model of earthquake ground motion

Following [46], a seismic ground motion $s(t)$ with $t \in [0, T]$ is modeled as:

$$s(t) = q(t, \boldsymbol{\alpha}) \left[\frac{1}{\sigma_f(t)} \int_{-\infty}^{t} h[t - \tau, \boldsymbol{\beta}(\tau)] w(\tau) d\tau \right], \tag{1}$$

where $q(t, \boldsymbol{\alpha})$ is a deterministic, non-negative modulating function that is defined piecewisely as

$$q(t, \boldsymbol{\alpha}) = \begin{cases} \alpha_1 t^2 / T_1^2 & \text{if} \quad 0 \leq t \leq T_1, \\ \alpha_1 & \text{if} \quad T_1 \leq t \leq T_2, \\ \alpha_1 \exp\left[-\alpha_2 (t - T_2)^{\alpha_3}\right] & \text{if} \quad T \geq t \geq T_2, \end{cases} \tag{2}$$

and that depends on the vector-valued parameter $\boldsymbol{\alpha} = (\alpha_1, \alpha_2, \alpha_3, T_1, T_2) \in \mathbb{R}_+^5$. The process inside the squared brackets of Eq. (1) is a filtered white-noise process of unit variance. $w(t)$ is a white-noise process and $h(t, \boldsymbol{\beta})$ is the Impulse Response Function (IRF) of the linear filter that depends on the vector-valued parameter $\boldsymbol{\beta}$. $\sigma_f^2(t) = \int_{-\infty}^{t} h^2(t - \tau, \boldsymbol{\beta}(\tau)) d\tau$ is the variance of the process defined by the integral in Eq. (1). In order to achieve spectral nonstationarity of the ground motion, the parameter $\boldsymbol{\beta}$ is allowed to depend on the time τ. Following [46], the IRF is of the form:

$$\begin{aligned} &h[t - \tau, \boldsymbol{\beta}(\tau)] \\ &= \frac{\omega_f(\tau)}{\sqrt{1 - \zeta_f^2}} \exp\left[-\zeta_f \omega_f(\tau)(t - \tau)\right] \sin\left[\omega_f(\tau)\sqrt{1 - \zeta_f^2}(t - \tau)\right] \mathbf{1}_{t \geq \tau}, \end{aligned} \tag{3}$$

where $\boldsymbol{\beta}(\tau) = [\omega_f(\tau), \zeta_f]$, $\omega_f(\tau)$ is the natural frequency (that depends on the time τ) and $\zeta_f \in [0, 1]$ is the (constant) damping ratio. A linear form is chosen for the frequency: $\omega_f(\tau) = \omega_0 + \frac{\tau}{T}(\omega_n - \omega_0)$. The IRF is, therefore, parameterized by $\boldsymbol{\lambda} = (\omega_0, \omega_n, \zeta_f) \in \mathbb{R}_+^3$.

The modulation parameters $\boldsymbol{\alpha}$ and the filter parameters $\boldsymbol{\lambda}$ are identified independently following the procedure proposed in [41, 46] for the $N_\mathrm{r} = 97$ acceleration records selected from the European Strong Motion Database [47] in the domain $5.5 < M < 6.5$ and $R < 20$km, where M is the magnitude and R the distance from the epicenter. The identification of the model parameters $\boldsymbol{\theta} = (\boldsymbol{\alpha}, \boldsymbol{\lambda})$ for each of the $N_\mathrm{r} = 97$ acceleration records, gives N_r data points $(\boldsymbol{\theta_i})_{i=1}^{N_\mathrm{r}}$ in the parameter space $\mathbb{R}_+^8$. The model then allows to generate artificial signals, thanks to the white-noise. However, these signals would all have very similar features due to the limited number of real signals considered to define the GMSM. In order to estimate fragility curves, a second level of randomness is added in the generation process, coming from the parameters $\boldsymbol{\theta}$ themselves. The parameters' probability distribution function can be estimated using a Gaussian Kernel Density Estimation (KDE) method [48]:

$$p_{KDE}(\boldsymbol{\theta}) = \frac{1}{N_\mathrm{r}} \sum_{i=1}^{N_\mathrm{r}} \phi_{\mathbf{H}}(\boldsymbol{\theta} - \boldsymbol{\theta_i}), \tag{4}$$

where $\phi_{\mathbf{H}}$ is a Gaussian kernel centered at 0 with covariance matrix $\mathbf{H}$ properly chosen from the data points $(\boldsymbol{\theta_i})_{i=1}^{N_\mathrm{r}}$ (see [48]). Finally, the simulation of an artificial ground motion requires three steps:

1. choose an integer $i \in [\![1, N_\mathrm{r}]\!]$ with a uniform distribution;
2. sample a vector $\mathbf{y}$ from a multivariate Gaussian distribution with probability density function $\phi_{\mathbf{H}}$, and let $\boldsymbol{\theta} = \boldsymbol{\theta_i} + \mathbf{y}$ (to be precise: reject the vector $\boldsymbol{\theta}$ if it does not belong to $\mathbb{R}_+^8$);
3. sample a realization of $w(t)$ and compute the signal with parameters $\boldsymbol{\theta} = (\boldsymbol{\alpha}, \boldsymbol{\lambda})$ by Eq. (1).

In this work $N_\mathrm{s} = 10^5$ artificial seismic ground motions $s_i(t)$ are generated.

2.2. Model of the mechanical structure

In order to illustrate the methodology, a nonlinear single degree of freedom system is considered. Despite its extreme simplicity, it reflects the essential features of the nonlinear responses of some real structures. In addition, in a probabilistic context requiring Monte Carlo simulations, it provides reference results at a reasonable numerical cost. Its equation of motion is:

$$\ddot{z}_i(t) + 2\beta\omega_\mathrm{L}\dot{z}_i(t) + f_i^{nl}(t) = -s_i(t), \quad i \in [\![1, N_\mathrm{s}]\!], \tag{5}$$

where $\dot{z}_i(t)$ and $\ddot{z}_i(t)$ are respectively the relative velocity and acceleration of the unit mass of the system submitted to the ith signal $s_i(t)$ with null initial conditions in velocity and displacement. In Eq. (5), β is the damping ratio, $\omega_\mathrm{L} = 2\pi f_\mathrm{L}$ is the circular frequency, and $f_i^{nl}(t)$ is the nonlinear resisting force. In this study, $f_\mathrm{L} = 5$ Hz, $\beta = 2\%$, the yield displacement is $Y = 5\,10^{-3}$ m, and the post-yield stiffness, defining kinematic hardening, is equal to 20% of the elastic stiffness. The relative displacement $\tilde{z}_i(t)$ of the Associated Linear System (ALS), assumed to be known in practice, is governed by the equation:

$$\ddot{\tilde{z}}_i(t) + 2\beta\omega_\mathrm{L}\dot{\tilde{z}}_i(t) + \omega_\mathrm{L}^2\tilde{z}_i(t) = -s_i(t). \tag{6}$$

Eqs. (5-6) are solved with a finite-difference method and we set:

$$Z_i = \max_{t\in[0,T]}|z_i(t)|, \tag{7}$$
$$L_i = \max_{t\in[0,T]}|\tilde{z}_i(t)|. \tag{8}$$

2.3. Choice of the seismic IM indicators

A complete review of the existing seismic IM indicators can be found in [19]. The methodology proposed here is intended to take into account the advantage of using a ground motion parametric model, in considering its constitutive parameters as input parameters of a metamodel. Thus, if $\mathcal{B} = (s_i(t))_{i\in[\![1,N_\mathrm{s}]\!]}$ is the database of N_s simulated ground motions, we can consider $\boldsymbol{\theta_i} = (\boldsymbol{\alpha}_i, \boldsymbol{\lambda}_i) \in \mathbb{R}_+^8$ the associated modulating and filter parameters as inputs. However, they can not be used alone since there is an infinity of possible realizations of the stochastic process for a set of parameters, due to the white-noise process. They have to be used additionally with the main classical IM parameters. Thus, for every signal $s_i(t)$, we also consider:

1. the Peak Ground Acceleration : $PGA_i = \max_{t\in[0,T]} |s_i(t)|$;
2. the Peak Ground Velocity : $V_i = \max_{t\in[0,T]} \left|\int_0^t s_i(\tau)d\tau\right|$;
3. the Peak Ground Displacement : $D_i = \max_{t\in[0,T]} \left|\int_0^t \int_0^\tau s_i(u)dud\tau\right|$;
4. the total energy $E_i = \int_0^T s_i^2(\tau)d\tau$ (this IM parameter is proportional to the "Arias Intensity" indicator usually considered);
5. the linear displacement L_i. The PSA $\omega_\mathrm{L}^2 L_i$ is usually considered as IM indicator, nevertheless, since the variable of interest is a nonlinear displacement, it is more suitable to use linear displacement. This structure-dependent indicator can be easily evaluated from the signal $s_i(t)$ and it improves the performance of the metamodeling strategy because it is strongly correlated with Z_i.

It is worth noting that the use of the classical IM indicators in association with the ground motion's ones does not guarantee that it is possible to find a perfect "meta-indicator", i.e. a perfect combination of the input indicators that can predict the failure of the structure with very high accuracy. In fact, this is not possible because, for a given value of PGA, there is an infinite number of possible realizations of the ground motion. This also applies to all IM indicators and this is the main challenge for this type of problem. Nevertheless, we will see that the proposed methodology allows efficient estimations of fragility curves with very good precision. So, each signal $s_i(t)$ is represented by a vector $\boldsymbol{X}_i^\star = (\boldsymbol{\alpha}_i, \boldsymbol{\lambda}_i, PGA_i, V_i, D_i, E_i, L_i) \in \mathbb{R}_+^{13}$ in order to predict whether the nonlinear displacement Z_i is greater than a damage state threshold, for example twice the yield displacement Y.

2.4. Discussion

Different GMSMs can be used to enrich a database of real seismic signals [23, 36, 37, 38, 39, 40], knowing that there is no consensus regarding the one which has to be privileged. To the best of the knowledge of the authors, if a generator is defined from real seismic signals, it is considered as valid if the statistical characteristics of the artificial signals are close to the ones of the real signals reduced to some scalar indicators (PGA, L, etc), and this is the case here. However, the influence of the GMSM is out of the scope of this work which aims to propose a general methodological framework to find an "optimal" classifier (or indicator) for a non-prohibitive computational cost, whatever the structure and the GMSM considered.

3. Binary Classification and Active Learning

In section 3.1, a simple but crucial preprocessing of the data is first addressed. Indeed, although the results of the comparative study are not shown here for the sake of brevity, this preprocessing improves the performance of the classifier. In sections 3.2-3.5, different classification methods and the active learning methodology are presented. The latter consists in selecting sequentially n signals $s_i(t)$ and computing the corresponding displacements Z_i (which is the time-consuming step) in order to build a classifier that will predict whether the displacement Z of a new signal $s(t)$ exceeds the threshold $2Y$. Finally, considering the structure presented in section 2.2, which allows calculations of N structural responses with a reasonable computational time, the performances of different classifiers are compared in sections 3.6-3.8. With $N \gg n$, this comparison is used to give recommendations on the values of n that can be considered in practice to estimate the fragility curves of complex structures (section 3.9).

3.1. Preprocessing of the training data

First of all, recall that $N_\mathrm{s} = 10^5$ signals have been generated and, for each of them, the displacement L_i of the ALS have been calculated. Signals with very small or very large values of L are discarded from the database. Indeed, on the one hand, the signals which produce values of L lower than the yield displacement Y are not useful, because the structural responses do not reach the limit threshold $2Y$: if $L_i < Y$, then $Z_i = L_i$ and thus $Z_i < Y$. This discards 66% of the N_s signals. On the other hand, the very few signals which produce very large values of L ($L_i > 6Y$) are also discarded because the

mechanical model is not realistic beyond that level. This gives a subset I of the database, composed of $N = 33718$ signals, such that $\forall i \in I$, $L_i \in [Y, 6Y]$. In addition, a Box-Cox transform is applied to each of the thirteen entries of $\boldsymbol{X}_i^\star = (\boldsymbol{\alpha}_i, \boldsymbol{\lambda}_i, PGA_i, V_i, D_i, E_i, L_i) \in \mathbb{R}_+^{13}$. This nonlinear step is critical for the accuracy of the classification, especially for linear SVM classifiers. The Box-Cox transform (parameterized by $\delta \in [0, +\infty)$) reads:

$$\mathrm{BC}_\delta(x) = \begin{cases} \dfrac{x^\delta - 1}{\delta} & \text{if } \delta \neq 0, \\ \log(x) & \text{if } \delta = 0. \end{cases} \tag{9}$$

The parameter δ is optimized, for each entry, in order to obtain an empirical distribution as close as possible to the normal law by maximizing the log-likelihood. Finally, all of the thirteen components are standardized, thus forming the training database $\boldsymbol{\mathcal{X}} = \{\boldsymbol{X_1}, \ldots, \boldsymbol{X_N}\}$ with $\boldsymbol{X_i} \in \mathbb{R}^{13}$.

3.2. Simple classifiers

At the most basic level, a binary classifier is a labeling function

$$\begin{array}{rcl} \hat{l} : \mathbb{R}^d & \longrightarrow & \{-1, 1\} \\ \boldsymbol{X} & \longmapsto & \hat{l}(\boldsymbol{X}), \end{array} \tag{10}$$

that, given a vector $\boldsymbol{X} \in \mathbb{R}^d$ (corresponding to a seismic signal $s(t)$), gives an estimated label $\hat{l}$. In this work, the true label l_i of instance $\boldsymbol{X_i}$ is 1 if the displacement Z_i is greater than the damage threshold $2Y$, and -1 otherwise:

$$l = \mathrm{sgn}(Z - 2Y) = \begin{cases} 1 & \text{if} \quad Z > 2Y, \\ -1 & \text{otherwise.} \end{cases} \tag{11}$$

Note that the true label l_i is not in general a function of the vector $\boldsymbol{X_i}$, since it depends on the full signal $s_i(t)$ when $\boldsymbol{X_i}$ only gives macroscopic measures of the signal; therefore, a perfect classifier $\hat{l}(\boldsymbol{X_i})$ may not exist (see section 2.3). One simple choice for a classifier is to look at only one component of the vector $\boldsymbol{X}$. For example, as the PGA is correlated with the nonlinear displacement Z, it can be used as a classifier defined by:

$$\hat{l}_{PGA}(\boldsymbol{X}) = \mathrm{sgn}(PGA - M), \tag{12}$$

where M is a threshold to be adjusted. Moving the threshold up results in less false positives ($\hat{l} = 1$ when the real label is $l = -1$) but more false

negatives ($\hat{l} = -1$ when the real label is $l = 1$); and moving the threshold down results in the opposite. There is therefore a choice of M such that the number of false positives and false negatives is equal. Note that this choice does not guarantee that the total number of misclassifications is minimal. Similarly, we can also define a classifier $\hat{l}_L$ based on the linear displacement L, since it is also highly correlated with the nonlinear displacement Z. These two simple classifiers give a baseline to assess the performance of advanced classifiers.

3.3. Support Vector Machines

In machine learning, SVMs are supervised learning models used for classification and regression analysis. In the linear binary classification setting, given a training data set $\{\boldsymbol{X_1}, \ldots, \boldsymbol{X_n}\}$ that are vectors in $\mathbb{R}^d$, and their labels $\{l_1, \ldots, l_n\}$ in $\{-1, 1\}$, the SVM is a hyperplane of $\mathbb{R}^d$ that separates the data by a maximal margin. More generally, SVMs allow one to project the original training data set $\{\boldsymbol{X_1}, \ldots, \boldsymbol{X_n}\}$ onto a higher dimensional feature space via a Mercer kernel operator K. The classifier then associates to each new signal $\boldsymbol{X}$ a score $f_n(\boldsymbol{X})$ given by $f_n(\boldsymbol{X}) = \sum_{i=1}^{n} \varphi_i K(\boldsymbol{X_i}, \boldsymbol{X})$. A new seismic signal represented by the vector $\boldsymbol{X}$ has an estimated label $\hat{l}$ of 1 if $f_n(\boldsymbol{X}) > 0$, -1 otherwise. In a general SVM setting, most of the labeled instances $\boldsymbol{X_i}$ have an associated coefficient φ_i equal to 0; the few vectors $\boldsymbol{X_i}$ such that $\varphi_i \neq 0$ are called "support vectors", hence the name "support vector machine". This historical distinction among labeled instances is less relevant in the case of active learning (see next section), since most of the φ_i are non-zero. In the linear case, $K(\boldsymbol{X_i}, \boldsymbol{X})$ is the scalar product in $\mathbb{R}^d$, and the score is:

$$f_n(\boldsymbol{X}) = \boldsymbol{W}^T \boldsymbol{X} + c, \tag{13}$$

where $\boldsymbol{W} \in \mathbb{R}^d$ and $c \in \mathbb{R}$ depend on the coefficients φ_i. Another commonly used kernel is the Radial Basis Function (RBF) kernel using Gaussian radial basis functions.

3.4. Active learning : basic principles

In the case of pool-based active learning, we have, in addition to the labeled set $\boldsymbol{\mathcal{L}} = \{\boldsymbol{X_1}, \ldots, \boldsymbol{X_n}\}$, access to a set of unlabeled samples $\boldsymbol{\mathcal{U}} = \{\boldsymbol{X_{n+1}}, \ldots, \boldsymbol{X_N}\}$ (therefore $\boldsymbol{\mathcal{X}} = \boldsymbol{\mathcal{L}} \cup \boldsymbol{\mathcal{U}}$). We assume that there exists a way to provide a label for any sample $\boldsymbol{X_i}$ from this set (in our case, running a full simulation of the physical model using signal $s_i(t)$), but the labeling cost is

high. After labeling a sample, we simply add it to the training set. In order to improve a classifier it seems intuitive to query labels for samples that cannot be easily classified. Various querying methods are possible [35, 49]. The method presented here only requires to compute the score $f_n(\boldsymbol{X})$ for the samples in the unlabeled set, then to identify a sample that reaches the minimum of the absolute value $|f_n(\boldsymbol{X})|$, since a score close to 0 means a high uncertainty for this sample. The algorithm starts with $n = 2$ samples with indices j_1 and j_2, labeled $+1$ and -1 (see next section). Recursively, if the labels of signals $j_1, \ldots, j_n$ are known, it consists in :

1. computing the SVM classifier associated with the labeled set $\{(\boldsymbol{X_{j_1}}, l_{j_1}), \ldots, (\boldsymbol{X_{j_n}}, l_{j_n})\}$;
2. computing the score $f_n(\boldsymbol{X_i})$ for each unlabeled instance $\boldsymbol{X_i}$, $i \in [\![1, N]\!] \backslash \{j_1, \ldots, j_n\}$;
3. identifying the instance with maximum uncertainty for this classifier:

$$j_{n+1} = \underset{i \in [\![1,N]\!] \backslash \{j_1,\ldots,j_n\}}{\operatorname{argmin}} |f_n(\boldsymbol{X_i})|, \tag{14}$$

   and computing the corresponding displacement $Z_{j_{n+1}}$ by running a full simulation of the mechanical model;
4. adding the instance $(\boldsymbol{X_{j_{n+1}}}, l_{j_{n+1}} = \operatorname{sgn}(Z_{j_{n+1}} - 2Y))$ to the labeled set.

No termination criteria are explicitly given here because, in practice, the limitation regarding the number of training data available is mainly due to the computational cost of the numerical mechanical calculations. The large number of simulations carried out here makes it possible to give recommendations on the required number of simulations (section 3.9).

3.5. Active learning : choice of the starting points

The active learner needs two starting points, one on each side of the threshold. After the preprocessing step, about 17% of the N remaining instances have a displacement greater than the threshold (although this precise value is usually unknown). It can be tempting to choose, for example, the signal with the smallest PGA as j_1 and the signal with the largest PGA as j_2. However, running simulations with these signals is costly and give a relatively useless information. We prefer to choose the starting points randomly, which also allows to see how this randomness affects the final performance of the classifier. As the parameters L_i and PGA_i of the ith signal are both

strongly correlated with Z_i, it is preferable that the starting points respect the order for these two variables:

$$Z_{j_1} < 2Y < Z_{j_2}, \quad L_{j_1} < L_{j_2}, \quad \text{and} \quad PGA_{j_1} < PGA_{j_2}. \tag{15}$$

Indeed, if j_1 and j_2 are such that, for example, $Z_{j_1} < 2Y < Z_{j_2}$ but $PGA_{j_1} > PGA_{j_2}$, then the active learner starts by assuming that the PGA and Z have negative correlation, and it can take many simulations before it "flips"; in some rare instances the classifier performs extremely poorly for several hundreds of simulations. Thus, the starting points j_1 and j_2 are chosen such that Eq. (15) is satisfied, using empirical quantiles of PGA and L. j_1 is chosen randomly among the instances whose PGA and L are smaller than their median values (i.e., their 0.5-quantiles $q_{0.5}(PGA)$ and $q_{0.5}(L)$):

$$j_1 \in \{i \in [\![1, N]\!] \quad | \quad PGA_i < q_{0.5}(PGA) \quad \& \quad L_i < q_{0.5}(L)\}. \tag{16}$$

It is almost certain that any instance in this set satisfies $Z_i < 2Y$ and thus $l_i = -1$. Similarly, j_2 is chosen using the 0.9-quantile $q_{0.9}(PGA)$ of PGA and the 0.9-quantile $q_{0.9}(L)$ of L:

$$j_2 \in \{i \in [\![1, N]\!] \quad | \quad PGA_i > q_{0.9}(PGA) \quad \& \quad L_i > q_{0.9}(L)\}. \tag{17}$$

In this case, the probability that $Z_i > 2Y$ is found to be 97%. So, if $Z_i < 2Y$, this signal has to be discarded in order to choose another one.

3.6. Performance checking : ROC curve and PRBP

Two tests of performance are proposed in this section. They are based on a large set of N nonlinear displacements Z, with $N \gg n$ and n the number of instances required by the active learning algorithm to train the classifier. In practice these tests are not possible (because of the prohibitive cost of the nonlinear displacements), but the model of mechanical structure described in section 2.2 makes it possible to compute them here.

The SVM classifier gives an estimated label $\hat{l}_i$ to each signal $s_i(t)$ depending on its score $\hat{l}_i = \text{sgn}(f_n(\boldsymbol{X_i}))$. As for the simple classifiers (section 3.2), the SVM classifier can be defined in terms of a real-valued limit $\beta \in \mathbb{R}$ by:

$$\hat{l}_i(\beta) = \text{sgn}(f_n(\boldsymbol{X_i}) - \beta). \tag{18}$$

If $\beta > 0$, then the number of false positives ($l_i = -1$ and $\hat{l}_i = 1$) is smaller, but the number of false negatives ($l_i = 1$ and $\hat{l}_i = -1$) is larger, relative to the

$\beta = 0$ case, and the opposite is true if we choose $\beta < 0$. Taking all possible values for $\beta \in \mathbb{R}$ defines the Receiver Operating Characteristic (ROC) curve. The area under the ROC curve is a common measure for the quality of a binary classifier. The classifier is perfect if there exists a value of β such that all estimated labels are equal to the true labels; in this case the area under the curve is equal to 1. Fig. 1 shows one example of active learning, with ROC curves for different numbers of labeled signals. As expected, the classifier improves when the labeled set gets larger; and the active learner becomes better than the simple PGA classifier as soon as $n \geq 10$.

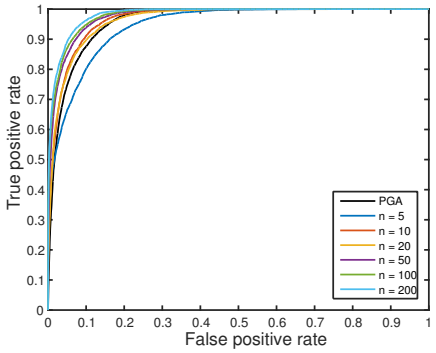

Figure 1: ROC curves for the PGA classifier (black) and for six active learners after n simulations ($n = 5, 10, 20, 50, 100$ and 200).

Another metric can be used to measure performance: the Precision/Recall Breakeven Point (PRBP) [49]. Precision is the percentage of samples a classifier labels as positive that are really positive. Recall is the percentage of positive samples that are labeled as positive by the classifier. By altering the decision threshold on the SVM we can trade precision for recall, until both are equal, therefore defining the PRBP. In this case the number of false positives and false negatives are equal. Let us denote by N_+ the number of instances where the displacement Z_i is greater than the threshold (on a total of N signals in the database):

$$N_+ = \#\left\{i \in [\![1, N]\!] \quad | \quad l_i = 1\right\}. \tag{19}$$

We sort all instances according to their score, i.e. we find a permutation σ such that $f_n(\boldsymbol{X}_{\sigma(1)}) \leq \cdots \leq f_n(\boldsymbol{X}_{\sigma(N)})$. Then the PRBP is equal to the proportion of positive instances among the N_+ instances with the highest

score:

$$\text{PRBP} = \frac{\#\left\{i \in [\![1, N]\!] \quad | \quad l_i = 1 \quad \& \quad \sigma(i) > N - N_+\right\}}{N_+}. \tag{20}$$

This criterium does not depend on the number of true negatives (unlike the false positive rate, used in the ROC curve). In particular, it is not affected by the choice of preprocessing of the training data, where all the weak signals ($L_i < Y$) are rejected. Both metrics are affected by the choice to discard the very strong signals ($L_i > 6Y$), but the effect is negligible in both cases.

3.7. Binary classification results for simple elasto-plastic structures

Considering the simple elasto-plastic structure presented in section 2.2, performances of different classifiers are compared considering the PRBP, in order to highlight the effectiveness of the active learning algorithm. More precisely, we compare different *orderings* of all signals, since only the order matters to the PRBP; for instance, the PGA does not give directly a label, but we can compute the PRBP of the PGA classifier with Eq. (20) using the permutation σ_{PGA} that sorts the PGA of all signals. Thus, we compare:

1. the simple PGA and L classifiers $\hat{l}_{PGA}$ and $\hat{l}_L$. These simple classifiers are defined with the $N = 33718$ signals and labels ;
2. ANNs trained with all instances and all labels (i.e. with the N signals and labels), with either all 13 parameters, or just 4 of them: (L, PGA, V, ω_0) (see section 3.8 for justification of this choice). The ANNs we use are full-connected Multi Layered Perceptrons (MLPs) with 2 layers of 26 and 40 neurons for $\boldsymbol{X} \in \mathbb{R}^4$, and two layers of 50 and 64 neurons for $\boldsymbol{X} \in \mathbb{R}^{13}$. This classifier is considered for completeness to show the best results we have achieved with the seismic indicators considered in $\mathbb{R}^4$ and in $\mathbb{R}^{13}$ with all the N instances;
3. SVMs given by the active learning algorithm (using a limited number n of instances).

Fig. 2 shows the PRBP of (i) a linear SVM using all thirteen parameters (in blue), (ii) a linear SVM using only four parameters (L, PGA, V, ω_0) (in red) and (iii) a RBF SVM, using the same four parameters (in yellow), as functions of the number n of labeled instances. As active learners depend on the choice of the first two samples, results of Fig. 2 are averaged over twenty pairs of starting points, the same starting points being used for all three types

of SVMs. In addtion, Fig. 2 shows the performances of four classifiers built using all the N signals. These four classifiers are represented as horizontal lines, since they do not depend on n. Fig. 2 shows that active learning gives a much better classifier than the standard practice based on a single parameter (PGA or L). The linear SVM with only four variables has initially the best performance on average, up to $n = 150$–200 simulations. The linear SVM with thirteen variables is better when $n \geq 200$. The RBF kernel in $\mathbb{R}^4$ appears to have the best performance with $n = 1000$, outperforming the ANNs in $\mathbb{R}^4$ using all N labeled instances. RBF SVMs with thirteen parameters seem to always perform very poorly, and are not represented here. So, in conclusion, (i) active learners need a minimum of $n = 30/40$ simulations, otherwise they can end up worse than using the simpler PGA classifier, (ii) between $n = 50$ and $n = 200$ simulations, the linear SVM in $\mathbb{R}^4$ is the best choice and (iii) the RBF kernel seems quite unpredictable for less than $n = 1000$ simulations (not shown here), and its performance strongly depends on the starting points, probably because of over-fitting. This methodology was applied to structures with different frequencies (not shown here for the sake of brevity) and the conclusions were similar.

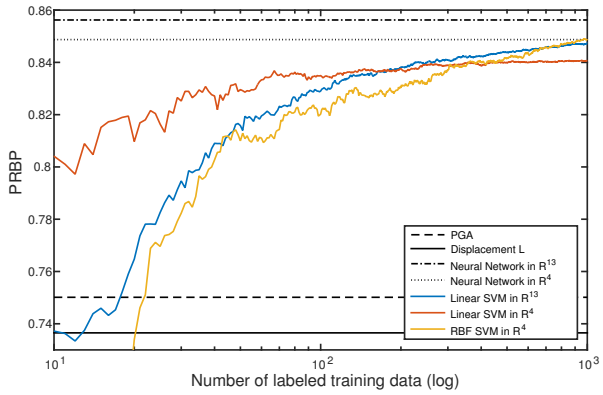

Figure 2: Performances of three active learning classifiers (averaged over twenty test cases) as functions of the number n of labeled instances, and comparison with classifiers using all $N = 33718$ instances.

3.8. Remark about the dimension reduction

In the linear case the score is equal to the distance to the hyperplane: $f_n(\boldsymbol{X}) = \boldsymbol{W}^T\boldsymbol{X} + c$ (Eq. (13)). Therefore, since the thirteen components of $\boldsymbol{X}$

are standardized in the preprocessing procedure (see section 3.1), it can be seen which of them are the most important for the classification by looking at the values of the components of $\boldsymbol{W}$. Fig. 3 shows that the values of $\boldsymbol{W}$ are roughly the same for the twenty test cases. After $n = 1000$ simulations, the coefficients for the PGA and L end up between 3 and 4, the value for V is around 1 and the value for the signal main frequency ω_0 is around -1. The other nine components of $\boldsymbol{W}$ (when working with $\boldsymbol{X} \in \mathbb{R}^{13}$) are all between -1 and 1, but are smaller (in absolute value) than these four components. As seen previously, reducing the dimension from thirteen to four allows for a faster convergence, although the converged classifier is less precise. Continuing the active learning after $n = 1000$ simulations changes only marginally the results; even with $\boldsymbol{X} \in \mathbb{R}^{13}$, both the PRBP and the values of $\boldsymbol{W}$ stay roughly the same between $n = 1000$ and $n = 5000$ simulations.

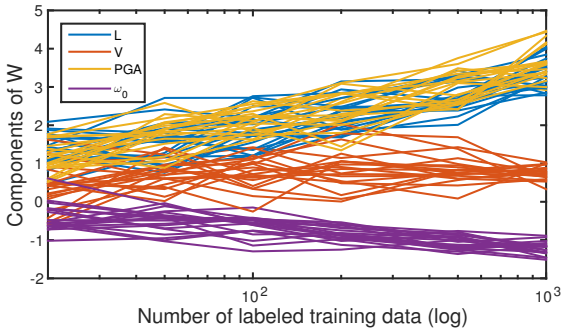

Figure 3: Evolution of the four main components of $\boldsymbol{W}$ for the twenty test cases.

3.9. Synthesis and Recommendations

Although the results are not shown here for the sake of brevity, (i) the simple preprocessing of the data presented in section 3.1 is necessary to improve the performances of the SVM classifiers especially when they are linear and (ii) the performances of the SVM classifiers are structure-dependent. The input parameters in $\mathbb{R}^4$ or in $\mathbb{R}^{13}$ are indeed more or less well correlated with the output according to the structure considered. Nevertheless, the proposed methodology is very general and can be applied to a variety of structures. The results show that a minimum of $n = 100$ simulations, selected via an active learning algorithm (sections 3.4 and 3.5), are necessary to obtain very precise classifiers. For $n = 100$ simulations, it is shown that linear SVM classifiers in $\mathbb{R}^4$ are sufficient. In this case, for the class of structures, the

seismic scenario and the GMSM considered, the main seismic IM parameters are the classical ones, i.e. PGA, V, L and ω_0. In the next section it is shown that such a classifier allows good estimations of fragility curves.

4. Fragility Curves

Different procedures can be used to construct non-parametric fragility curves [3, 21, 23]. Here, they are constructed based on k-means clustering of the IM data [23]. In a Monte Carlo-based approach this means that in each cluster, the empirical probability of failure is evaluated by the ratio between the number of structural responses that exceed the limit threshold and the number of structural responses belonging to the cluster. With SVM classifiers which give to each signal $s_i(t)$ a real-valued score $f_n(\boldsymbol{X_i})$ whose sign expresses the estimated label, we first need to assign a probability to estimate fragility curves. In this section we explain how SVMs can be used to estimate fragility curves, using either the score functions (which can be viewed as an optimal seismic IM since a perfect classifier would lead to a fragility curve in the form of a unit step function when the problem is linearly separable) or IM indicators such as the PGA or the PSA (replaced here by L).

4.1. Fragility curves estimations

The estimation of the score-based fragility curve is based on a probabilistic interpretation of the output of the SVM. The probabilistic interpretation of the SVM output depends only on the score $f_n(\boldsymbol{X})$. For a perfect classifier, the probability would be 0 if $f_n(\boldsymbol{X}) < 0$ and 1 if $f_n(\boldsymbol{X}) > 0$; for the SVM classifiers a logistic function is used in order to get a probablity in $(0, 1)$:

$$p_n(\boldsymbol{X}) = \frac{1}{1 + \exp[-a f_n(\boldsymbol{X}) + b]}, \tag{21}$$

where a and b are the slope and intercept parameters of the logistic function (b should be close to 0 if the classifier has no bias, giving a probability of $1/2$ to signals with $f_n(\boldsymbol{X}) \approx 0$). These parameters are estimated by maximizing the likelihood function from Eq. (21) on the labeled set $\{(\boldsymbol{X_{j_1}}, l_{j_1}), \ldots, (\boldsymbol{X_{j_n}}, l_{j_n})\}$.

The estimation of the score-based fragility curve is given by Eq. (21). If we are interested in more-understandable fragility curve such as PGA-based fragility curve (or an other IM-based fragility curve), the classifier should first be used to predict the scores and the associated probabilities by Eq. (21) of several new input parameters. These new input parameters correspond to

those which were not selected for the construction of the classifier, or other ones generated from new simulations of the GMSM. Then, as in a Monte Carlo-based approach, k-means clustering has to be used on the IM indicator of interest. In each cluster, the probability of failure is then evaluated by averaging the probabilities associated to the input parameters belonging to the cluster.

4.2. Score-based fragility curve

To compare the estimation given by Eq. (21) with the empirical failure probability of signals $s_i(t)$, the set of indices $\{1, \dots, N\}$ of the database $\boldsymbol{\mathcal{X}}$ is divided into K groups $(I_1, \dots, I_K)$ depending on their score $f_n(\boldsymbol{X_i})$, with the k-means algorithm. Then, the estimated p_k^{est} and reference p_k^{ref} probabilities are defined in each group by:

$$\begin{array}{rcl} p_k^{est} & = & \frac{1}{n_k} \sum_{i \in I_k} p_n(X_i), \\ p_k^{ref} & = & \frac{1}{n_k} \#\left\{ i \in I_k | l_i = 1 \right\}, \end{array} \qquad \text{with} \quad n_k = \#I_k. \tag{22}$$

The L_2 distance between these two probabilities is given by:

$$\Delta_{L_2} = \sqrt{\frac{1}{N} \sum_{k=1}^{K} n_k (p_k^{ref} - p_k^{est})^2}, \qquad \text{with } N = \sum_{k=1}^{K} n_k. \tag{23}$$

Fig. 4 shows the L_2 distance for different classifiers using $n = 20, 50, 100, 200, 500$ and 1000 labeled instances. The three classifiers (linear SVM in $\mathbb{R}^{13}$, linear SVM in $\mathbb{R}^4$, and RBF kernels in $\mathbb{R}^4$) are compared considering twenty pairs of starting points. The solid lines show the average L_2 errors, and the dashed lines show the minimum and maximum errors among all test cases. The average error goes down from 15% after $n = 20$ simulations to less than 3% after $n = 1000$ simulations for the linear SVM in $\mathbb{R}^{13}$, and from 9% to less than 2% for the linear SVM in $\mathbb{R}^4$. For RBF kernels (in yellow), the average error does not decrease as n increases, and ends up around 20% after $n = 1000$ simulations.

Fig. 5 shows examples of fragility curves obtained with each method after $n = 1000$ simulations. Recall that the logistic functions (in red) are not fitted using all the real data (in blue), but only the labeled set, i.e. $n = 1000$ signals. The linear SVM in $\mathbb{R}^4$ has the least errors in terms of probabilities, although its PRBP is smaller than that of the linear SVM in $\mathbb{R}^{13}$. The RBF kernel shows an unintuitive result. Indeed, the probability of failure is not an

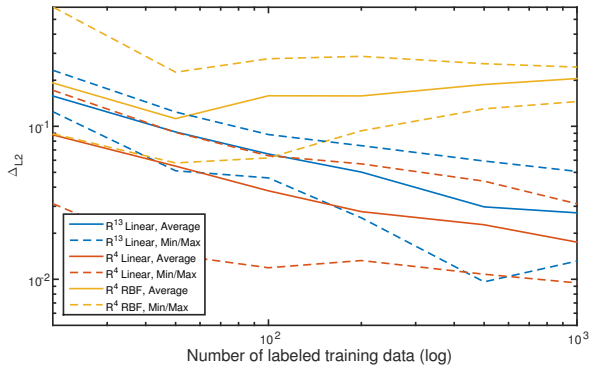

Figure 4: Distance Δ_{L_2} for the three different active learners.

increasing function of the score (Fig. 5c); in particular, signals with a very negative score still have a 5–10% chance of exceeding the threshold. This result explains why the Δ_{L_2} error of RBF kernels is so high (Fig. 4), since we have tried to fit a logistic curve on a non-monotonous function.

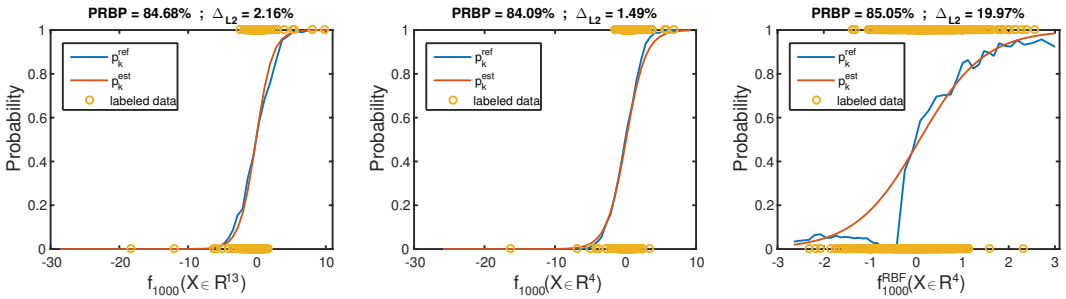

(a) (b) (c)

Figure 5: Reference and estimated score-based fragility curves using (a) a linear SVM in $\mathbb{R}^{13}$, (b) a linear SVM in $\mathbb{R}^4$ and (c) a RBF SVM in $\mathbb{R}^4$ with $n = 1000$ labeled instances.

The reason for this major difference between linear and RBF kernels can be understood if we look at the nonlinear displacement Z as a function of the score $f_n(\boldsymbol{X})$, using both kernels (see Fig. 6). Let us keep in mind that the RBF classifier at $n = 1000$ simulations is the most precise of all our active learners; it has the fewest false positives and false negatives of all (Table 1 in red). The sign of the RBF score is thus an excellent predictor for binary classification.

linear kernel	$f_n(\boldsymbol{X}) < 0$	$f_n(\boldsymbol{X}) > 0$
$Z > 2Y$	1020	4711
$Z < 2Y$	27175	812

RBF kernel	$f_n(\boldsymbol{X}) < 0$	$f_n(\boldsymbol{X}) > 0$
$Z > 2Y$	1009	4722
$Z < 2Y$	27287	700

Table 1: Confusion matrix for linear SVM in $\mathbb{R}^4$ and RBF SVM in $\mathbb{R}^4$ with $n = 1000$.

Fig. 6 shows that for the linear classifier, the score is a good predictor of the nonlinear displacement Z, with a monotonous relation between the two; therefore the probability that $Z > 2Y$ can be well-approximated by a logistic function of the score. The RBF score is a poor predictor of the probability of failure, since the relation between the score and the nonlinear displacement Z is not monotonous. This explains why the Δ_{L_2} errors for RBF kernels are very high. In Fig. 6, we can see that the weakest signals ($Z = 0.005$, just above Y) have a RBF score between -1 and -0.4. Since these weak signals are very common in the database, p_k^{ref} goes rapidly from 0.5 for $f_n^{\mathrm{RBF}}(\boldsymbol{X}) = 0$ to almost 0 for $f_n^{\mathrm{RBF}}(\boldsymbol{X}) = -0.5$ (Fig. 5c), not because the number of positive signals changes significantly between $f_n^{\mathrm{RBF}}(\boldsymbol{X}) = -0.5$ and $f_n^{\mathrm{RBF}}(\boldsymbol{X}) = 0$, but because the number of negative signals is more than twenty times larger. The linear kernels do not have this problem and have much lower Δ_{L_2} errors.

ROC curves (Fig. 7) give a further insight into the dilemma between the two kernels. If we look at the unbiased (i.e. $\beta = 0$) classifiers, the RBF is slightly superior: it has fewer false positives and slightly fewer false negatives than the linear classifier. However, for a negative limit β (Eq. (18)), for example $\beta = -0.5$, some of the weakest signals end up over the limit ($f_{1000}^{\mathrm{RBF}}(\boldsymbol{X}) > \beta$) and thus have an estimated label of $\hat{l}(\beta) = 1$. Since these weak signals are so common, the false positive rate becomes extremely high.

4.3. PGA-based and L-based fragility curves

In the previous section the score $f_n(\boldsymbol{X})$ has been used as the parameter on the x-axis to build the fragility curves. The method assigns a probability $p_n(\boldsymbol{X})$ to each signal, depending only on a few parameters. If we consider this probability as a function of four parameters ($p_n(L, V, PGA, \omega_0)$ if $\boldsymbol{X} \in \mathbb{R}^4$), then any of those parameters can be used to define *a posteriori* a fragility

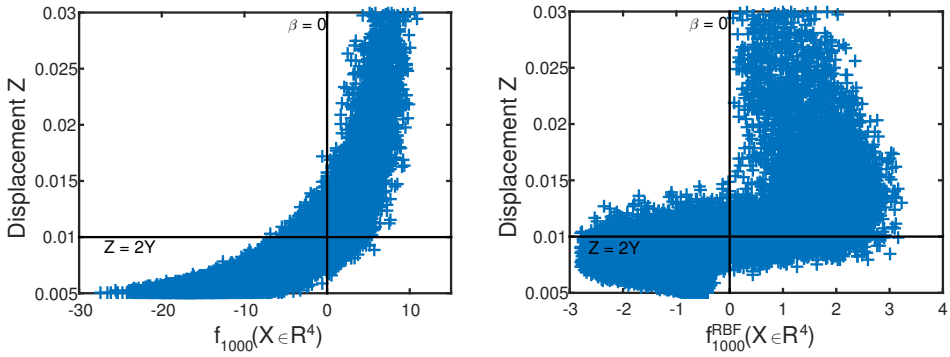

(a) (b)

Figure 6: Nonlinear displacment Z as a function of the score given after $n = 1000$ simulations by (a) the linear SVM in $\mathbb{R}^4$ and (b) the RBF SVM in $\mathbb{R}^4$.

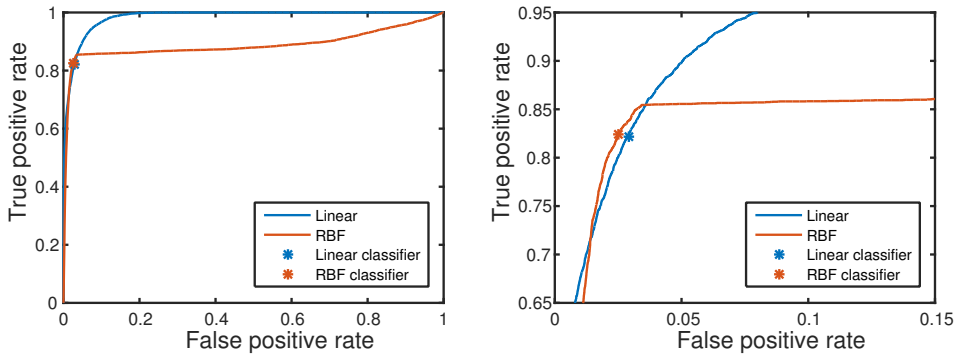

(a) (b)

Figure 7: (a) ROC curves for two SVM classifiers using linear and RBF kernels, with specific values for the unbiased (i.e. $\beta = 0$) classifiers. (b) zoom on the upper-left corner.

curve depending on this parameter, averaging over the other ones:

$$p_n(PGA) = \mathbb{E}[p_n(\boldsymbol{X})|PGA]. \tag{24}$$

In practice, to obtain numerically the corresponding estimated and reference probabilities, we use k-means algorithm, and divide the database into K groups $(I_1, \ldots, I_K)$ depending on their PGA (resp. on their L), instead of the score, then compute p_k^{est} and p_k^{ref} using Eq. (22). Figs. 8 and 9 show two examples of such curves, using PGA or L ; $p_n(\boldsymbol{X})$ is computed using a

linear SVM classifier in $\mathbb{R}^4$ with $n = 100$ or $n = 1000$ simulations. In this case, all twenty test cases are shown in a single figure, since they share a common x-axis (which is not true when the score is used). The distance between the reference and estimated curves is small in all cases, even with $n = 100$ labeled instances.

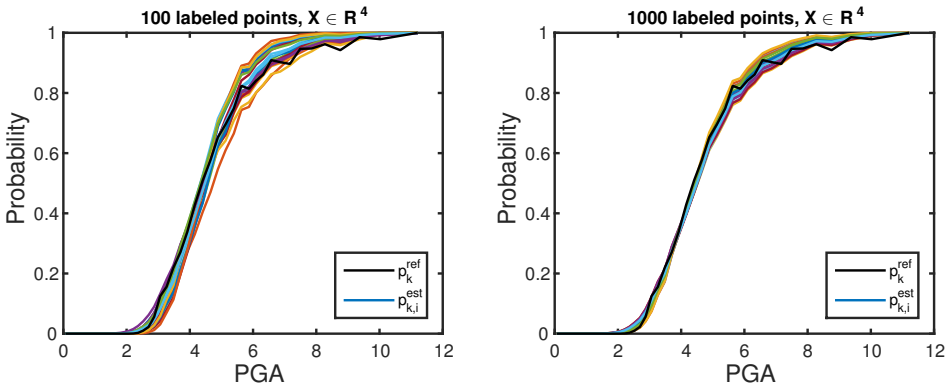

(a) (b)

Figure 8: Reference and estimated fragility curves as a function of PGA, using (a) $n = 100$ and (b) $n = 1000$ labeled points.

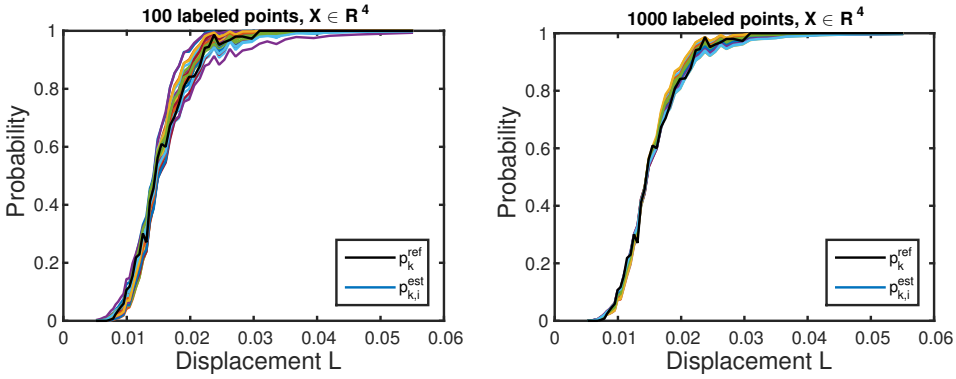

(a) (b)

Figure 9: Reference and estimated fragility curves as a function of L, using (a) $n = 100$ and (b) $n = 1000$ labeled points.

4.4. Trading precision for steepness

The PGA-based and L-based fragility curves (Figs. 8 and 9) are very close to the reference curves; the distance Δ_{L_2} between the reference and estimated curves is very small, even smaller than in the case of score-based fragility curves. In this case, what is the benefit of score-based fragility curves compared to more-understandable PGA-based curves ? The difference is in the steepness of the curve. Formally, when we construct a fragility curve, we choose a projection $F : \mathbb{R}^4 \mapsto \mathbb{R}$ to use as the x-axis. This projection $F(\boldsymbol{X})$ can be one of the 4 variables (e.g. the PGA), or the score $f_n(\boldsymbol{X})$, which can be a linear or nonlinear (in the case of RBF kernel) combinaison of the four variables. We then use the k-means algorithm to make K groups of signals which are close according to this projection, i.e. signals with the same PGA, the same L or the same score; then we compute the estimated probability p_k^{est} for each group. Let us assume for a while that the estimation is very precise, so that $p_k^{est} = p_k^{ref}\ \forall k$. In this case, which fragility curve gives the most information ? To see this, we define:

$$R^{(F)} = \frac{1}{N} \sum_{k=1}^{K} n_k \phi(p_k^{est}) \tag{25}$$

for some nonnegative-valued function ϕ. Intuitively, a perfect classifier would give each signal a probability of 0 or 1, while a classifier which assigns a probability of 1/2 to many signals is not very useful. Therefore, we want ϕ to be positive on $(0, 1)$, equal to 0 for $p = 0$ and $p = 1$. We choose the entropy-like function:

$$\phi(p) = -p \ln(p), \tag{26}$$

so that $R^{(F)}$ is equal to 0 for a perfect classifier and has higher values for a useless classifier. Other suitable choices could be $\phi(p) = p(1 - p)$ or $\phi(p) = \mathbf{1}_{p \in [0.1, 0.9]}$. In the latter case, $R^{(F)}$ has a clear physical meaning: it is the proportion of uncertain signals, i.e. signals such that $p_k^{est} \in [0.1, 0.9]$. Table 2 shows the value of $R^{(F)}$ using the entropy version, for different choices of projection (score, PGA, or L). We can see in this table that the PGA- and L-based fragility curves are extremely precise, with very low values of Δ_{L_2} (this can also be seen in Figs. 8 and 9), but their entropy is much higher than the score-based fragility curves.

One surprising fact of Table 2 is that the entropy is smaller at $n = 100$ compared to $n = 1000$ in all three cases. This shows that after only $n = 100$

	projection	score	PGA	L
$n = 100$	Δ_{L_2} (%)	3.8 ± 1.6	2.6 ± 1	2.8 ± 0.9
	entropy (10^{-2})	5.3 ± 1.7	12.3 ± 1.8	12.2 ± 2
$n = 1000$	Δ_{L_2} (%)	1.7 ± 0.6	1.6 ± 0.3	1.4 ± 0.4
	entropy (10^{-2})	7.2 ± 1.2	13.3 ± 1.5	13.6 ± 1

Table 2: Precision and entropy of fragility curves using different projections (average and standard deviation over 20 test cases), for $n = 100$ or $n = 1000$ labeled points.

mechanical calculations, all the classifiers tend to slightly overestimate the steepness, and give fragility curves that are actually steeper than the reality (and also steeper than the more realistic curves obtained with $n = 1000$). Using the other choices of function $\phi(p)$ gives the same conclusions: the proportion of signals with $p_k^{est} \in [0.1, 0.9]$ is 18.2% if the score is used instead of 28% for PGA and L. Therefore, the choice of the projection used for a fragility curve is a trade-off between precision and steepness. Note that the values of the entropy for different choices of projection can be obtained after the active learning, and the computationnal cost is very small (mostly the cost of k-means). As a consequence, this choice can be made a posteriori, from the probabilities assigned to each signal.

5. Conclusion

This paper proposes an efficient methodology for estimating non-parametric seismic fragility curves by active learning with a SVM classifier. We have introduced and studied this methodology when aleatory uncertainties have a predominant contribution in the variability of structural response, that is to say when the contribution of uncertainties regarding seismic excitation is much larger than the contribution of uncertainties regarding structural capacity. In this work, the structure is considered as deterministic and a perfect classifier, if it exists, would lead to a fragility curve in the form of a unit step function, i.e. corresponding to a fragility curve "without uncertainty". That means the output of this classifier, which is a real-valued score, would be the best seismic IM indicator to evaluate the damaging potential of the seismic signals, knowing that such a classifier would necessary be both structure and failure criterion-dependent, with possibly a dependence on the ground motion characteristics (near-fault type like, broadband, etc).

The proposed methodology makes it possible to build such a (non perfect) classifier. It consists in (i) reducing the input excitation to some relevant parameters and, given these parameters, (ii) using a SVM for a binary classification of the structural responses relative to a limit threshold of exceedance. Selection of the mechanical numerical calculations by active learning dramatically reduces the computational cost of construction of the classifier. The output of the classifier, the score, is the desired IM indicator which is then interpreted in a probabilistic way to estimate fragility curves as score functions or as functions of classical seismic IMs.

This work shows that a simple and universal preprocessing of the data (Box-Cox transformation of the input parameters) makes it possible to use a simple linear SVM to obtain a very precise classifier after only one hundred mechanical calculations. Moreover, it shows that the input parameters of the GMSM can be used additionally to the classical IM parameters to build the classifier and to improve its performance. For the class of structures considered, with only four classical seismic parameters (PGA, V, L, ω_0), the score-based fragility curve is very close to the reference curve (obtained with a direct Monte Carlo-based approach) and steeper than the PGA-based one, as expected. L-based fragility curves appear to perform about as well as PGA-based ones in our setting. Advanced SVMs using RBF kernel result in less classification errors when using one thousand mechanical calculations, but do not appear well suited to making fragility curves.

Acknowledgements

This research was supported by the French National Research Agency (grant ANR CHORUS MONU-0005), by CEA (French Alternative Energies and Atomic Energy Commission) and SEISM Institute (www.institut-seism.fr/en/).

References

[1] R. P. Kennedy, C. A. Cornell, R. D. Campbell, S. Kaplan, and H. F. Perla. Probabilistic seismic safety study of an existing nuclear power plant. *Nuclear Engineering and Design*, 59(2):315–338, 1980. 2

[2] Ahmed Ghobarah. Performance-based design in earthquake engineering: state of development. *Engineering Structures*, 23(8):878–884, 2001. 2

[3] Hae Young Noh, David Lallemant, and Anne S. Kiremidjian. Development of empirical and analytical fragility functions using kernel smoothing methods. *Earthquake Engineering & Structural Dynamics*, 44(8):1163–1180, 2105. 2, 5, 18

[4] Jian Zhang and Yili Huo. Evaluating effectiveness and optimum design of isolation devices for highway bridges using the fragility function method. *Engineering Structures*, 31(8):1648–1660, 2009. 2

[5] Sandip Kumar Saha, Vasant Matsagar, and Subrata Chakraborty. Uncertainty quantification and seismic fragility of base-isolated liquid storage tanks using response surface models. *Probabilistic Engineering Mechanics*, 43:20–35, 2016. 2

[6] Atul Patil, Sungmoon Jung, and Oh-Sung Kown. Structural performance of a parked wind turbine tower subjected to strong ground motions. *Engineering Structures*, 120:92–102, 2016. 2

[7] Ioannis Gidaris, Alexandros A. Taflanidis, and George P. Mavroeidis. Kriging metamodeling in seismic risk assessment based on stochastic ground motion models. *Earthquake Engineering & Structural Dynamics*, 44(14):2377–2399, 2015. 2, 3

[8] Sabarethinam Kameshwar and Jamie E. Padgett. Storm surge fragility assessment of above ground storage tanks. *Structural Safety*, 70:48–58, 2018. 2, 3

[9] Fan Wang and Cyril Feau. Influence of Input Motion's Control Point Location in Nonlinear SSI Analysis of Equipment Seismic Fragilities: Case Study on the Kashiwazaki-Kariwa NPP. *Pure and Applied Geophysics*, 2020. 2

[10] Esteban Sáez, Fernando Lopez-Caballero, and Arézou Modaressi-Farahmand-Razavi. Effect of the inelastic dynamic soil–structure interaction on the seismic vulnerability assessment. *Structural Safety*, 33(1):51–63, 2011. 2

[11] Charlie Mathey, Cyril Feau, David Clair, Laurent Baillet, and Michel Fogli. Experimental and numerical analyses of variability in the responses of imperfect slender free rigid blocks under random dynamic excitations. *Engineering Structures*, 172:891–906, 2018. 2

[12] A. Quilligan, A. O'Connor, and V. Pakrashi. Fragility analysis of steel and concrete wind turbine towers. *Engineering Structures*, 36:270–282, 2012. 2

[13] Bruce R. Ellingwood and Kursat Kinali. Quantifying and communicating uncertainty in seismic risk assessment. *Structural Safety*, 31(2):179–187, 2009. Risk Acceptance and Risk Communication. 2

[14] Armen Der Kiureghian and Ove Ditlevsen. Aleatory or epistemic? does it matter? *Structural Safety*, 31(2):105–112, 2009. 2

[15] Masanobu Shinozuka, M. Q. Feng, Jongheon Lee, and Toshihiko Naganuma. Statistical analysis of fragility curves. *Journal of Engineering Mechanics*, 126(12):1224–1231, 2000. 2

[16] Baker Jack W. Efficient analytical fragility function fitting using dynamic structural analysis. *Earthquake Spectra*, 31:579–599, 2015. 2

[17] Vitor Silva, Helen Crowley, and Paolo Bazzurro. Exploring risk-targeted hazard maps for europe. *Earthquake Spectra*, 32(2):1165–1186, 2016. 2

[18] Tushar K. Mandal, Siddhartha Ghosh, and Nikil N. Pujari. Seismic fragility analysis of a typical indian PHWR containment: Comparison of fragility models. *Structural Safety*, 58:11–19, 2016. 2

[19] M.A. Hariri-Ardebili and V.E. Saouma. Probabilistic seismic demand model and optimal intensity measure for concrete dams. *Structural Safety*, 59:67–85, 2016. 2, 3, 8

[20] I. Zentner. Numerical computation of fragility curves for NPP equipment. *Nuclear Engineering and Design*, 240(6):1614–1621, 2010. 2

[21] Chu Mai, Katerina Konakli, and Bruno Sudret. Seismic fragility curves for structures using non-parametric representations. *Frontiers of Structural and Civil Engineering*, 11(2):169–186, Jun 2017. 2, 4, 5, 18

[22] Irmela Zentner. A general framework for the estimation of analytical fragility functions based on multivariate probability distributions. *Structural Safety*, 64:54–61, 2017. 2

[23] Konstantinos Trevlopoulos, Cyril Feau, and Irmela Zentner. Parametric models averaging for optimized non-parametric fragility curve estimation based on intensity measure data clustering. *Structural Safety*, 81:101865, 2019. 2, 4, 5, 9, 18

[24] Joonam Park and Peeranan Towashiraporn. Rapid seismic damage assessment of railway bridges using the response-surface statistical model. *Structural Safety*, 47:1–12, 2014. 3

[25] Junwon Seo and Daniel G. Linzell. Use of response surface metamodels to generate system level fragilities for existing curved steel bridges. *Engineering Structures*, 52:642–653, 2013. 3

[26] Zhiyi Wang, Nicola Pedroni, Irmela Zentner, and Enrico Zio. Seismic fragility analysis with artificial neural networks: Application to nuclear power plant equipment. *Engineering Structures*, 162:213–225, 2018. 3

[27] Nicolas Luco and C. Allin Cornell. Structure-specific scalar intensity measures for near-source and ordinary earthquake ground motions. *Earthquake Spectra*, 23(2):357–392, 2007. 3

[28] Kevin Mackie and Božidar Stojadinović. Probabilistic seismic demand model for california highway bridges. *Journal of Bridge Engineering*, 6(6):468–481, 2001. 3

[29] Paolo Giovenale, C. Allin Cornell, and Luis Esteva. Comparing the adequacy of alternative ground motion intensity measures for the estimation of structural responses. *Earthquake Engineering & Structural Dynamics*, 33(8):951–979, 2004. 3

[30] Jack W. Baker and C. Allin Cornell. Vector-valued intensity measures incorporating spectral shape for prediction of structural response. *Journal of Earthquake Engineering*, 12(4):534–554, 2008. 3

[31] Jamie E. Padgett, Bryant G. Nielson, and Reginald DesRoches. Selection of optimal intensity measures in probabilistic seismic demand models of highway bridge portfolios. *Earthquake Engineering & Structural Dynamics*, 37(5):711–725, 2008. 3

[32] M. Hasenjäger and H. Ritter. Active learning in neural networks. In Lakhmi C. Jain and Janusz Kacprzyk, editors, *New Learning Paradigms*

in Soft Computing, pages 137–169, Heidelberg, 2002. Physica-Verlag HD. 4

[33] H. S. Seung, M. Opper, and H. Sompolinsky. Query by committee. In *Proceedings of the Fifth Annual Workshop on Computational Learning Theory*, COLT '92, pages 287–294, New York, NY, USA, 1992. ACM. 4

[34] S. Gazut, J.-M. Martinez, G. Dreyfus, and Y. Oussar. Towards the optimal design of numerical experiments. *Trans. Neur. Netw.*, 19(5):874–882, 2008. 4

[35] Simon Tong and Daphne Koller. Support vector machine active learning with applications to text classification. *J. Mach. Learn. Res.*, 2:45–66, 2002. 4, 12

[36] Sanaz Rezaeian and Armen Der Kiureghian. A stochastic ground motion model with separable temporal and spectral nonstationarities. *Earthquake Engineering & Structural Dynamics*, 37(13):1565–1584, 2008. 4, 9

[37] Fabio Sabetta and Antonio Pugliese. Estimation of response spectra and simulation of nonstationary earthquake ground motions. *Bulletin of the Seismological Society of America*, 86(2):337, 1996. 4, 9

[38] S. Levy and J.P.D. Wilkinson. Generation of artificial time-histories, rich in all frequencies, from given response spectra. *Nuclear Engineering and Design*, 38(2):241–251, 1976. 4, 9

[39] Guillaume Pousse, Luis Fabian Bonilla, Fabrice Cotton, and Ludovic Margerin. Nonstationary stochastic simulation of strong ground motion time histories including natural variability: Application to the k-net japanese database. *Bulletin of the Seismological Society of America*, 96(6):2103, 2006. 4, 9

[40] Irmela Zentner and Fabrice Poirion. Enrichment of seismic ground motion databases using karhunen–loève expansion. *Earthquake Engineering & Structural Dynamics*, 41(14):1945–1957, 2012. 4, 9

[41] Sanaz Rezaeian and Armen Der Kiureghian. Simulation of synthetic ground motions for specified earthquake and site characteristics. *Earthquake Engineering & Structural Dynamics*, 39(10):1155–1180, 2010. 4, 5, 6

[42] N. Simon Kwong and Anil K. Chopra. Evaluation of the exact conditional spectrum and generalized conditional intensity measure methods for ground motion selection. *Earthquake Engineering & Structural Dynamics*, 45(5):757–777, 2016. 4

[43] J. A. Bachmann, M. Strand, M. F. Vassiliou, M. Broccardo, and B. Stojadinović. Is rocking motion predictable? *Earthquake Engineering & Structural Dynamics*, 47(2):535–552, 2018. 4

[44] Alexandra Tsioulou, Alexandros A. Taflanidis, and Carmine Galasso. Modification of stochastic ground motion models for matching target intensity measures. *Earthquake Engineering & Structural Dynamics*, 47(1):3–24, 2018. 4

[45] Michalis F. Vassiliou, Stefan Burger, Marius Egger, Jonas A. Bachmann, Marco Broccardo, and Bozidar Stojadinovic. The three-dimensional behavior of inverted pendulum cylindrical structures during earthquakes. *Earthquake Engineering & Structural Dynamics*, 46(14):2261–2280, 2017. 4

[46] Rezaeian Sanaz. *Stochastic modeling and simulation of ground motions for performance-based earthquake engineering*. PhD thesis, University of California, Berkeley, 2010. 5, 6

[47] N.N. Ambraseys, P. Smit, R. Berardi, D. Rinaldis, F. Cotton, and C. Berge. Dissemination of european strongmotion data, 2000. CD-ROM collection. European Commission, Directorate-General XII, Environmental and Climate Programme, ENV4-CT97-0397, Brussels, Belgium. 6

[48] Matej Kristan, Aleš Leonardis, and Danijel Skočaj. Multivariate online kernel density estimation with gaussian kernels. *Pattern Recognition*, 44(10):2630–2642, 2011. 6, 7

[49] Jan Kremer, Kim Steenstrup Pedersen, and Christian Igel. Active learning with support vector machines. *Wiley Int. Rev. Data Min. and Knowl. Disc.*, 4(4):313–326, 2014. 12, 14